Shi *et al. Carbon Research* (2022) 1:7
https://doi.org/10.1007/s44246-022-00006-4

Carbon Research

ORIGINAL ARTICLE

Open Access

Thermal stabilization effect and oxygen replacement reaction together regulate N/S co-doped microporous carbon synthesis

Shanshan Shi[1,2], Chao Jia[2,3], Xiaoyu Huo[1,2], Shicheng Zhang[2,3], Qunjie Xu[1*] and Xiangdong Zhu[2,4*]

Abstract

Potassium thiocyanate (KSCN) activation showed great potential to prepare N/S co-doped microporous carbon for environmental remediation, however, predictable preparation for targeted application was a challenge. This study suggested that thermal stabilization effect and oxygen replacement reaction during KSCN activation could together regulate pore formation and N/S co-doping. Results showed that carbonaceous precursor with high thermal stability (expressed by high R_{50} index) could support stable carbon matrix for KSCN pore-forming. Meanwhile, carbonaceous precursor with high polarity (expressed by high O/C) was more prone to occur oxygen replacement reaction, promoting N/S co-doping. N/S co-doped microporous carbon with high micropore surface area can promote BPA adsorption via the pore-filling mechanism. However, reaction induced by S contained groups can enhance heavy metal (Pb^{2+}) adsorption while prepared material with S doping. In summary, a carbonaceous precursor with high R_{50} index was conducive to preparing carbon material for organic pollutant adsorption, while the carbonaceous precursor with high O/C was suit to fabricate carbon material with high adsorption capacity for Pb^{2+} immobilization. This study provided important insights into the directional synthesis of optimized N/S doped microporous carbon.

Highlights

1) Thermal stabilization effect in KSCN activation regular micropore of carbon material.

2) Oxygen replacement in KSCN activation regular N/S doping of carbon material.

3) High R_{50} precursor was suit to prepare material for organic pollutant adsorption.

4) High O/C precursor was suit to prepare carbon material for Pb^{2+} immobilization.

Keywords: N/S doped microporous carbon, Thermal stabilization effect, Oxygen replacement reaction, Adsorption

Graphical Abstract

*Correspondence: xuqunjie@shiep.edu.cn; zxdjewett@fudan.edu.cn

[1] College of Environmental & Chemical Engineering, Shanghai University of Electric Power, Shanghai 200090, China
[2] Shanghai Technical Service Platform for Pollution Control and Resource Utilization of Organic Wastes, Shanghai Key Laboratory of Atmospheric Particle Pollution and Prevention (LAP3), Department of Environmental Science and Engineering, Fudan University, Shanghai 200438, China
Full list of author information is available at the end of the article

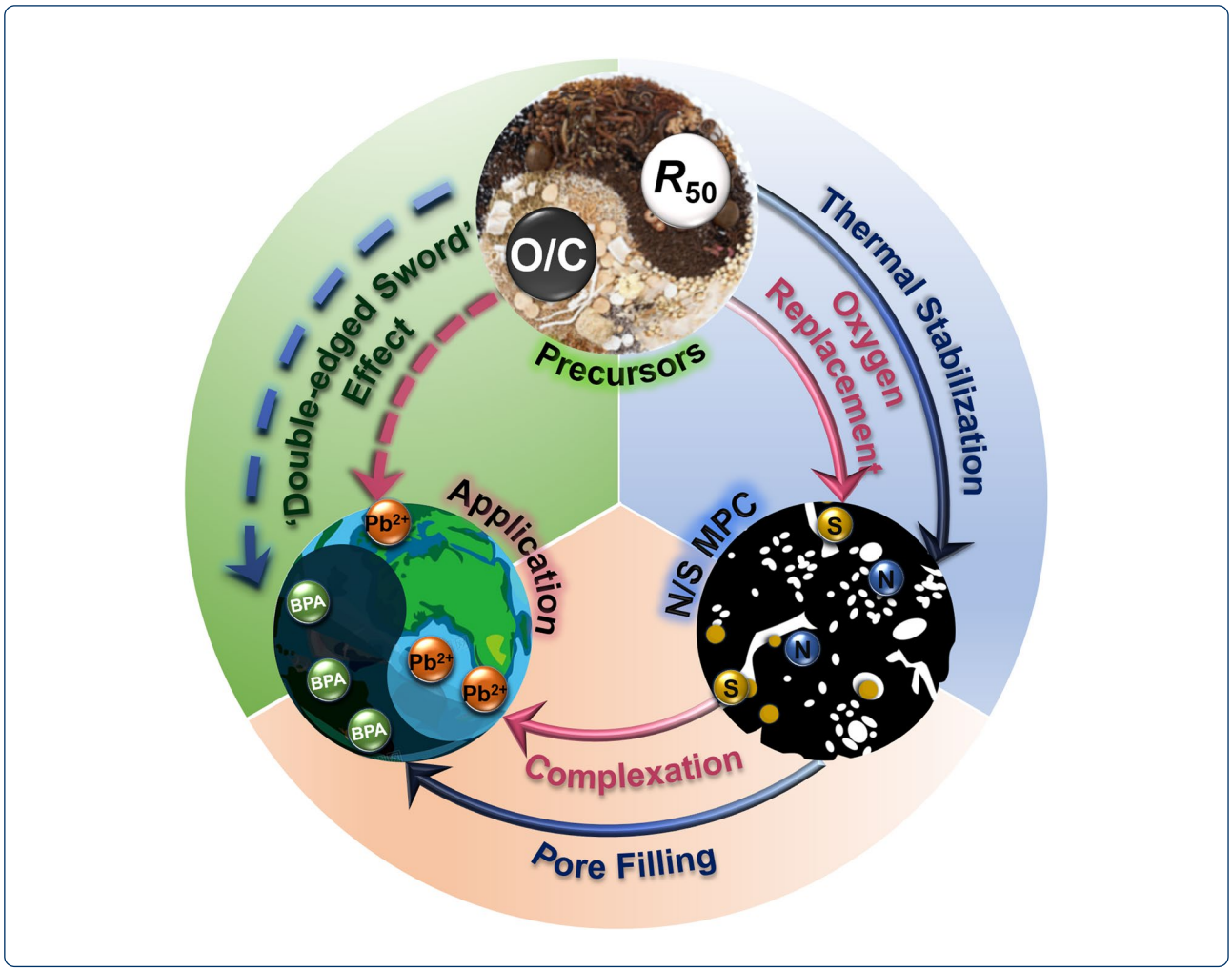

1 Introduction

At present, nitrogen and sulfur doped microporous carbons are known as very effective adsorbents in the field of environmental pollution control due to their developed porosity and variable surface chemical characteristics (Gao et al. 2015; Sun et al. 2020; Tian et al. 2016a, b). According to previous studies, N-doping enhanced the electronic properties and improved the hydrophobic characteristics of carbon materials, while S-doping induced high chemical reactivity (Kasera et al. 2022; Liang et al. 2012). The pore filling of microporous structure and the complexation of N functional groups contribute to the immobilization of organic compounds on carbon materials (Ahamad et al. 2019; Luo et al. 2019). For example, Luo et al. fabricated N-doped carbon with high BET surface area (3046 m^2/g) and N content (10.8%), which exhibited high BPA adsorption capacity (909 mg/g) (Luo et al. 2019). In addition, effective S are essential for improving the heavy metal adsorption due to the complexation. Jia et al. reported that N/S-co-doped microporous carbon with high S content (10.9%) could effectively remove Pb^{2+} from wastewater (Jia et al. 2021).

In recent years, the preparation methods of N/S doped carbon materials were mainly divided into two categories: (i) the organic precursors rich in N and S were directly pyrolyzed without activator (Gao et al. 2015; Ma et al. 2019; Zhou et al. 2016) and (ii) the pore forming agent was combined with organic dopants (such as urea, melamine or thiourea) to prepare carbon materials (Tan et al. 2018; Tian et al. 2016a, b). However, these two methods brought some disadvantages, such as low doping efficiency of heteroatoms and the need to add excessive dopants, resulting in high investment and energy consumption. Our recent research found that potassium thiocyanate (KSCN) could be used as both porogen and N/S dopant in the preparation of N/S co-doped microporous carbon materials (Jia et al. 2021). Research results confirmed that KSCN realized pore formation by activation reaction and

efficiency N/S co-doping by oxygen replacement reaction ($2KSCN + C_xH_yO_z \rightarrow K_2SO_4 + C_{x+2}H_yO_{z-4}N_2S$).

At present, the synthesis approaches of carbon materials with target properties depended on trial and error, preparing predictable material was a challenge. Biomass and its derived carbon materials were considered as renewable precursors of carbon materials because of their abundant content and sustainability in the environment (Hu et al. 2020; Maliutina et al. 2021; Xiong et al. 2021). Previous studies had proposed that carbonaceous precursors properties strongly affected the as-prepared carbon materials physicochemical properties, which would finally affect its application performance (Adeleye et al. 2021; Alsewaileh et al. 2019; Lu et al. 2019; Teong et al. 2021). Therefore, it is necessary to further study the influence mechanism of carbonaceous precursor on the structure and adsorption properties of N/S doped microporous carbon, so as to directly synthesize carbon materials with specific applications.

For this purpose, N/S co-doped microporous carbons were prepared from different carbonaceous precursors by KSCN activation method and used for BPA and Pb^{2+} adsorption. The influence mechanism of carbonaceous precursors properties (including thermal stability and polarity) on the properties (including surface area density, microporous surface area and N/S doping amount) of N/S co-doped microporous carbon was explored. The adsorption mechanism of BPA and Pb^{2+} on N/S co-doped microporous carbon was also discussed. Finally, based on the relationship between carbonaceous precursors properties and the adsorption capacity of N/S doped microporous carbon, the adaptability of raw materials to the target application was judged.

2 Materials and methods

2.1 Carbonaceous precursor for KSCN activation

Cellulose (CL), walnut shell (WS), sawdust (SD) and sawdust derived biochar with different thermal stability abilities and elemental compositions were used for KSCN activation. Walnut shell and sawdust were collected from rural areas in Shanghai. Cellulose powder and other reagents were purchased from Shanghai Aladdin Biochemical Technology Co., Ltd. Pyrolysis derived biochar was prepared in a tube furnace at a heating rate of 10 °C/min to 300 °C with a N_2 atmosphere. Air flow carbonization derived biochar was synthesized by heating to 300 °C or 400 °C in a N_2 atmosphere, then exposed to a flow of air for 10 min, after which the sample was cooled under a flow of nitrogen gas. Sawdust derived biochar prepared in this way was named *N-X* and *A-X*, where *X* represented the reaction temperature, *N* represented the sample activated in a nitrogen atmosphere and *A* represented the sample activated in air atmosphere.

Hydrothermal carbonization (HTC) derived biochar was prepared at a 1: 20 weight ratio between sawdust and deionized water in an autoclave with 180 °C or 300 °C heating temperature for 2 h. After the reaction, the products were washed with deionized water several times and dried overnight at 80 °C. The prepared hydrochar was represented by *H-X*, and *X* was the HTC experimental temperature (°C).

2.2 Preparation N/S co-doped microporous carbon materials by KSCN activation

Cellulose, walnut shell, sawdust and sawdust derived biochar with various properties were chemically activated by KSCN to prepare N/S doped microporous carbon. The mixture of carbonaceous precursor and KSCN at 1:1 weight ratio was activated at 700 °C for 90 min under 100 mL/min N_2 flow with a 10 °C/min heating rate in a tube furnace. The carbonized samples were then washed by 2 M HCl and deionized water to nature pH. The samples were finally being dried to constant weight in an oven at 100 °C.

2.3 Characterizations of carbonaceous precursor and N/S co-doped microporous carbon

Elemental and thermogravimetric analyses were used to characterize the carbonaceous precursor. Elemental composition (C, H, N, S) was analyzed with an elemental analyzer (Vario EL III). The ash content was measured by heating the sample in an air atmosphere at 600 °C for 2 h. Specifically, the O/C molar ratio was used to estimate the polarity of carbonaceous precursors. In order to quantitatively calculate the thermal stability of carbonaceous precursor, TG analysis in air atmosphere was carried out with heating from 30 ~ 800 °C at a rate of 10 °C/min by a thermogravimetric analyzer (SDT Q600). The thermal stability of carbonaceous precursor indicated by R_{50} index was quantitatively calculated as follows (Harvey et al. 2012),

$$R_{50} = \frac{T_{50,\ \text{precursor}}}{T_{50,\text{graphite}}}$$

where $T_{50,\ \text{precursor},}$ and $T_{50,\ \text{graphite}}$ were the temperature values corresponding to 50 % weight loss by oxidation and volatilization of carbonaceous precursor and graphite, respectively. The values of $T_{50,\ \text{precursor}}$ and $T_{50,\ \text{graphite}}$ were obtained directly from TG thermograms corrected for water and ash content. A more detailed account for the calculation of R_{50} was given in previous literature by Harvey et al. (2012).

The characterization of the N/S co-doped microporous carbon was done using N_2 adsorption/desorption, elemental analyzer, powder X-ray diffraction (XRD),

X-ray photoelectron spectroscopy (XPS) and Raman spectra. The surface area and porosity of N/S doped carbons were conducted on a Quantachrome Autosorb iQ2 instrument with N_2 adsorption/desorption isotherms at −196 °C. The specific surface area (S_{BET}) and total pore volume (V_T) were determined by the Brunauer-Emmett-Teller (BET) equation. Micropore surface area (S_{mic} < 2 nm) was calculated via the *t*-plot analysis. Pore size distribution was evaluated via density functional theory (DFT) method (Zhu et al. 2015). The crystal structure of unwashed activated samples was performed by powder X-ray diffraction (XRD) with Cu Kα radiation at 40 kV, 40 mA in the 2θ range of 10–80° (X' Pert PRO, Nalytical, Netherlands). Raman spectra were carried out using a XploRA Raman spectrometer with a 532 nm laser source, and the parameters were fitted five distinctive Gaussian peaks, corresponding to G (~ 1580 cm^{-1}), D (~ 1350 cm^{-1}), I (~ 1220 cm^{-1}), D′ (~ 1620 cm^{-1}) and D″ (~ 1490 cm^{-1}) bands. The O, N and S-containing functional groups of activated samples were determined by X-ray photoelectron spectroscopy (XPS) technique (Thermo ESCALAB 250 XI). In detail, the O 1 s spectra (including C = O, C-O-C and COOH), the N 1 s spectra (including pyridinic N, pyrrolic N, quaternary N, and oxidized N) and S 2p spectra (including C-SO_2, C-SO_3, C-S-C $2p_{1/2}$, and C-S-C $2p_{3/2}$) in the activated samples were fitted by the deconvolution method. The binding energies of high resolutions spectra were calibrated at C 1 s of 284.6 eV.

2.4 Adsorption experiments

Organic pollutant (bisphenol A, BPA) and heavy metal (Pb^{2+}) were selected to explore the water purification ability of N/S doped microporous carbon. For BPA adsorption isotherms, 3 mg material was dispersed in 30 mL BPA solution with different initial concentrations (2 ~ 200 mg/L). The mixture was shaken at 150 rpm for 12 h until adsorption equilibrium. The supernatant was filtered using a 0.45 μm polytetrafluoroethylene (PTFE) membrane filter to analyze the BPA concentration. The filtrate was measured by a UV–visible spectrometer (CARY 300, Agilent, USA) at 280 nm absorbance. In addition, the adsorption kinetics was achieved at 2, 5, 10, 30, 60, 120, 240, 480 min in the concentration of 150 mg/L BPA and 100 mg/L N/S co-doped microporous carbon at 25 °C. The adsorption isotherms were fitted to the Langmuir model and the adsorption kinetics were interpreted by the pseudo-second-order model, as detailed in our previous work (Zhu et al. 2014a, b).

In Pb^{2+} adsorption, 20 mg material was added in 40 mL Pb^{2+} solution with different initial concentrations (20 ~ 600 mg/L). 10 mM MES solution was used to stabilize the solution pH at about 5. The solution was continuously stirred at 150 rpm for 12 h to reach adsorption equilibrium and then the filtrates were measured by using Inductively Coupled Plasma-Atomic Emission Spectrometry (ICP-AES, Hitachi P4010) to determine the resultant Pb^{2+} concentration. The transmission electron microscopy (TEM, Tecnai G2 F20 S-Twin, FEI) and X-ray photoelectron spectroscopy (XPS, Thermo ESCALAB 250 XI) were used to characterize the Pb-adsorbed N/S co-doped microporous carbon to explore the adsorption mechanism.

3 Results and discussion

3.1 Thermal stability and polarity of carbonaceous precursor

Pyrolysis, air flow carbonization and hydrothermal carbonization were selected for carbonizing the raw sawdust into biochar, and the sawdust derived biochar together with cellulose, walnut shell and sawdust were used as activated carbonaceous precursors. The aim was to achieve carbonaceous precursors with different thermal stability (expressed by R_{50} index) and polarity (indicated by O/C). Based on previous study (Hirst et al. 2018; Zhu et al. 2015), pyrolysis, air flow carbonization and HTC increased the thermal stability ability of samples but reduced O/C. Moreover, the changes increased with the rise in reaction temperature.

As shown in Table 1, the R_{50} index was in a wide range of 0.3 ~ 0.53, and the value of *A-300* (from air flow carbonization at 300 °C) was the largest, indicating that it had strongest thermal stability, while cellulose had weakest. These conclusions showed that the biochar derived from high reaction temperature had stronger thermal resistance. In addition, compared with the O/C of untreated precursors, the O/C of carbonized precursors decreased. The *A-400* with the lowest O/C was derived from air flow carbonization and high reaction temperature, consistent with the conclusion that the carbonization process reduced the O content and increased the C content of carbon materials (Balahmar et al. 2017; Balahmar and Mokaya 2019; Hirst et al. 2018; Zhu et al. 2015). In addition, all carbonaceous precursors contain almost little N/S element (Table S1).

3.2 Porosity and doping evolution of N/S doped microporous carbon

Table 2 provided the yields, pore structure characteristics and element composition of N/S doped microporous carbon. As expected, N/S co-doped microporous carbon had high BET surface area (832 ~ 1532 m^2/g) and pore volume (0.46 ~ 1.21 cm^3/g). As shown in Fig. S1, the N_2 adsorption isotherm of all samples exhibited type I, revealing the presence of a large number of microporous structures. And the pore size distribution of N/S doped

Table 1 Ash contents, elemental compositions, and R_{50} index of different carbonaceous precursors

Sample	Ash (%)	C (%)	H (%)	O (%)	R_{50}	O/C[1]
CL[a]	0.00	44.4	6.17	49.4	0.30	1.11
WS[b]	1.67	48.2	4.69	45.2	0.37	0.70
SD[c]	0.62	50.0	7.52	41.9	0.33	0.63
H-180[d]	2.58	51.5	6.45	39.5	0.34	0.57
N-300[e]	1.76	59.9	4.00	34.3	0.50	0.43
A-300[f]	1.29	62.3	5.77	30.6	0.53	0.37
H-300[g]	0.85	68.9	5.10	24.9	0.50	0.27

[1] Mole ratio of oxygen to carbon

[a] Cellulose, [b]Walnut shell, [c]Sawdust, [d]Sawdust-derived hydrochar prepared at 180 °C, [e]Sawdust-derived biochar prepared at 300 °C in N_2 atmosphere, [f]Sawdust-derived biochar prepared at 300 °C in air atmosphere and [g]Sawdust-derived hydrochar prepared at 300 °C

Table 2 Elemental compositions and textural properties of different N/S doped microporous carbon

Sample	ID[a]	Yield (%)	C (%)	O (%)	N (%)	S (%)	S_{BET}[b] (m^2/g)	V_t[c] (cm^3/g)	SAD[d] (m^2/cm^3)	S_{mic}[e] (m^2/g)
NSC-CL	*A*	30	58.9	19.4	5.28	14.4	832	0.86	967	654 (79)
NSC-WS	*B*	39	66.7	12.7	5.25	13.0	1247	0.84	1485	1051 (84)
NSC-SD	*C*	37	64.0	16.4	4.87	13.2	1532	1.21	1266	1068 (70)
NSC-H-180	*D*	44	65.1	15.8	4.88	12.4	1422	1.09	1305	1095 (77)
NSC-N-300	*E*	58	63.7	19.0	4.66	11.1	1495	0.78	1907	1330 (89)
NSC-A-300	*F*	60	69.9	12.5	4.97	10.8	1507	0.78	1932	1293 (86)
NSC-H-300	*G*	84	67.7	15.7	5.12	9.98	1465	0.67	2187	1354 (92)

[a] Code name of different N/S doping microporous carbon, [b]BET surface area, [c]total pore volume and [d]surface area density (BET surface area / total pore volume) and [e]micropore surface area, the values in parenthesis was the S_{mic}/S_{BET} and the unit was %

microporous carbons was mainly about 1 ~ 2 nm, which indicated that the samples were microporous materials. Based on the previous study (Altwala and Mokaya 2020), the surface area density (the ratio between BET surface area and pore volume) was a parameter that defined porosity and measure the sensitivity of carbonaceous substances to activation. The high surface area density of porous materials was usually produced by the preponderance of micropores. Therefore, the higher the surface area density, the more micropores of carbon materials. As shown in Table 2, the surface area density of N/S co-doped microporous carbon was changed within the range from 967 to 2187 m^2/cm^3. The results of elemental analysis showed that the prepared material possessed similar N (4.66 ~ 5.28%) but various S (9.43 ~ 14.44%) doping ability.

3.2.1 Thermal stabilization effect criterion

The literature had well documented that the thermal stability of carbonaceous precursors affected the formation of pore structure in carbon materials (Harvey et al. 2012; Zhu et al. 2015). High surface area density indicated that more micropores in N/S co-doped microporous carbon materials. The positive linear correlation between the surface area density of N/S co-doped microporous carbon and R_{50} index of the carbonaceous precursors ($R^2 = 0.89$, Fig. 1a) proved that the carbonaceous precursor with high R_{50} was conducive to the formation of developed micropores. This was because that unstable carbonaceous precursor was easy to volatilize and lack of effective carbon matrix for pore-forming. The carbonaceous precursor with high R_{50} occurred intense thermal stabilization effect, more carbon matrix was better activated by KSCN to form micropores. High graphitization degree corresponded to high activation degree. The increased graphitization degree (expressed in reduced I_D/I_G value) of N/S co-doped microporous carbon with the increased R_{50} further proved that carbonaceous precursors with high R_{50} were easier to be activated (Fig. 2b and S2a). In a word, the different degrees of thermal stabilization effect occurred during the activation of the carbonaceous precursor by KSCN regulated the pore structure in N/S doped microporous carbon. The stronger the thermal stabilization effect, the more micropores in N/S doped microporous carbon. In addition, the positive linear correlation between the microporous surface area of N/S co-doped microporous carbon and R_{50} index of the carbonaceous precursors ($R^2 = 0.72$) indicated that the N/S co-doped microporous carbon materials produced

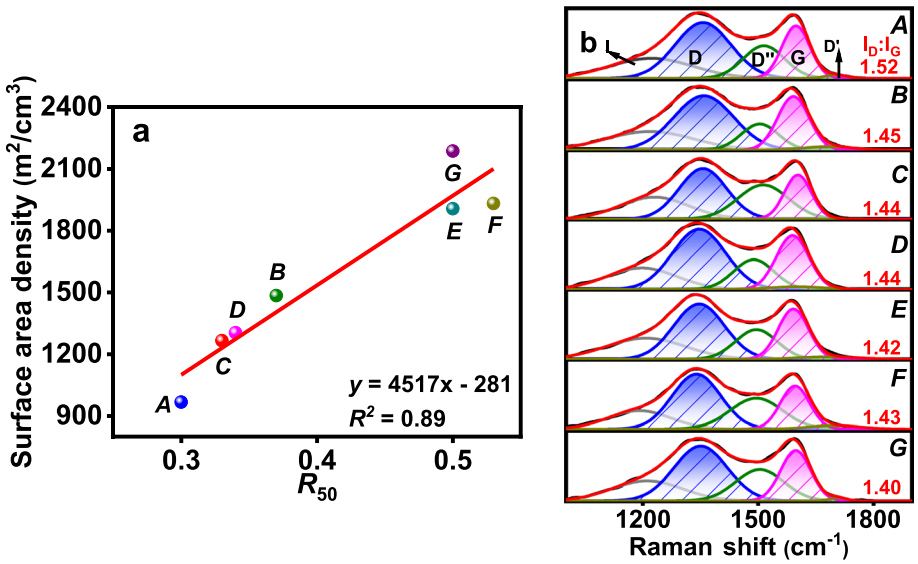

Fig. 1 **a** Linear correlation between the R_{50} index of carbonaceous precursors and the surface area density (defined as the ratio between total surface area and total pore volume) of N/S co-doped microporous carbon and **b** Raman spectrum of N/S co-doped microporous carbon was fitted using the five Gaussian peaks (color lines) (*A*: *NSC-CL*, *B*: *NSC-WS*, *C*: *NSC-SD*, *D*: *NSC-H-180*, *E*: *NSC-N-300*, *F*: *NSC-A-300*, *G*: *NSC-H-300*)

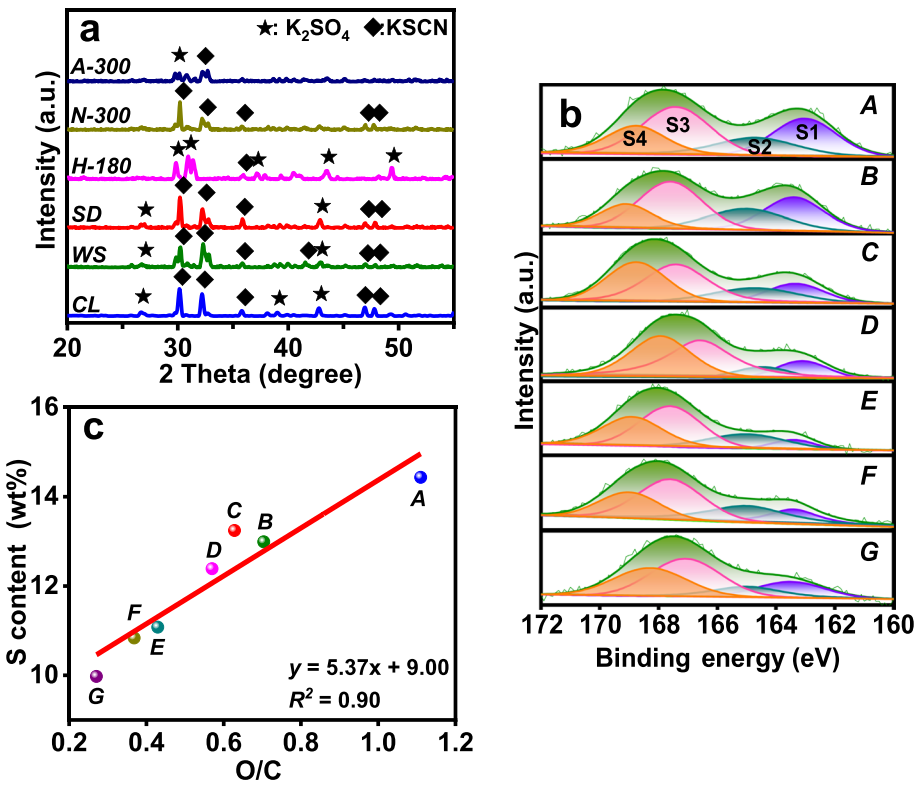

Fig. 2 **a** XRD patterns of the unwashed N/S doped microporous carbon, **b** S_{2p} spectra of N/S co-doped microporous carbon (S1: C-S-C $2p_{3/2}$, S2: C-S-C $2p_{1/2}$, S3: C-SO_2 S4: C-SO_3) and **c** linear correlation between the O/C of carbonaceous precursors and the S content of N/S co-doped microporous carbon (*A*: *NSC-CL*, *B*: *NSC-WS*, *C*: *NSC-SD*, *D*: *NSC-H-180*, *E*: *NSC-N-300*, *F*: *NSC-A-300*, *G*: *NSC-H-300*)

by carbonaceous precursors with high thermal stability had high micropore surface area (Fig. S2b).

3.2.2 Oxygen replacement reaction criterion

The existence of K_2SO_4 in unwashed N/S co-doped microporous carbon indicated that oxygen replacement reaction occurred during the carbonaceous precursor activated by KSCN (Fig. 2a). As a result, O in carbonaceous precursor can be substituted by S and N heteroatoms from KSCN, the generated S and N can be doped into the carbon materials. Three peaks were observed in representative N/S co-doped microporous carbon (*NSC-CL*) by deconvolution of O1s spectra, including C=O (531.3 eV), C-O-C (532.3 eV) and COOH (533.5 eV) (Fig. S3). And Four peaks, including pyridinic N, pyrrolic N, quaternary N, and oxidized N, were observed in the N/S doped microporous carbons via deconvolution of N 1 s spectra (Fig. S4). The deconvolution spectrum of S 2p showed that O can complex with S to form sulfur-oxygen functional groups (C-SO_2 and C-SO_3, Fig. 2b). The above results indicated that N was mainly doped on the carbon skeleton, while S could complex with O to improve the stability. Therefore, it should be noted that N and S had different sensitivities to heating, S was more stable during the reaction, while N would further occurred thermally decompose. This lead the contents of N and S in the carbon showed different trends, and the N contents were similar in various carbon precursors. The strong positive linear relationship observed between the S content of N/S doped microporous carbons and O/C of carbonaceous precursors (R^2 = 0.90, Fig. 2c) indicated that carbonaceous precursors with high O/C were more prone to occur oxygen replacement reaction in the KSCN activation. Meanwhile, the oxygen replacement reaction could adjust the S content in carbon materials, so the higher the content of S in N/S co-doped microporous carbon materials prepared from carbon precursor with high polarity.

As described above, the thermal stabilization effect and oxygen replacement reaction could together regulate the synthesis of N/S doped microporous carbon, especially affecting the surface area density, micropore surface area and S doping ability of carbon materials. Carefully selecting the carbonaceous precursors and clarifying the mechanism of their properties affecting the properties of N/S doped carbon were conducive to the directional synthesis of carbon materials with target functions.

3.3 N/S co-doped microporous carbon for water purification

BPA and Pb^{2+} were selected as typical pollutants to explore the water purification ability of N/S co-doped microporous carbon materials. The adsorption kinetic and isotherms experiments of BPA for N/S co-doped microporous carbon in aqueous solution were demonstrated in Fig. S5 and the calculated parameters were shown in Table S2. Results indicated that the adsorption equilibrium time was about 60 min (Fig. S5a). The results of isothermal adsorption showed that the maximum adsorption capacity of N/S co-doped microporous carbon materials for BPA reached 714 mg/g, indicating that N/S co-doped microporous carbon had excellent removal ability for BPA in aqueous solution.

Figure S6 showed that the q_{BET} of N/S co-doped microporous carbon materials was higher than that of porous carbon, indicating that N doping could improve the adsorption performance. Due to the similar content of N in prepared carbon materials, we did not conduct further correlation analysis of N. As shown in Fig. 3a, a positive correlation (R^2 = 0.97) between micropore surface area and BPA maximum adsorption capacity indicated that materials with high micropore surface area

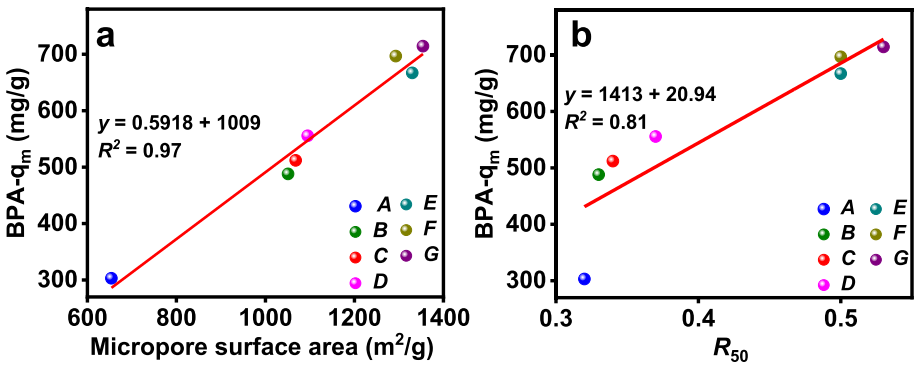

Fig. 3 **a** Linear correlation between BPA-q_m and micropore surface area of N/S co-doped microporous carbon and **b** linear correlation between R_{50} of carbonaceous precursors and BPA-q_m of N/S co-doped microporous carbon (*A*: *NSC-CL*, *B*: *NSC-WS*, *C*: *NSC-SD*, *D*: *NSC-H-180*, *E*: *NSC-N-300*, *F*: *NSC-A-300*, *G*: *NSC-H-300*)

usually correspond to high adsorption performance, which may be dependent on the pore-fitting mechanism (Luo et al. 2019). Further, a positive correlation can be observed between the R_{50} of carbonaceous precursor and the adsorption performance of N/S doping microporous carbon materials for BPA (Fig. 3b). This result showed that the carbonaceous precursor with high R_{50} was suitable for the preparation of N/S co-doped microporous carbon materials with strong adsorption capacity for BPA.

Adsorption isotherm experiment results of Pb^{2+} onto prepared materials were shown in Fig. S7a. Using the Langmuir model to fit the adsorption isotherm, it can be seen that the maximum adsorption capacity of N/S co-doped microporous carbon for Pb^{2+} varies from 286 mg/g to 357 mg/g (Table S3). Interestingly, a positive correlation (R^2 =0.78) was observed between S content of N/S co-doped microporous carbon and maximum adsorption capacity for Pb^{2+} (Fig. 4a). Meanwhile, the N content of N/S co-doped microporous carbon prepared from different carbonaceous precursors was stable. It was speculated that Pb^{2+} was fixed by complexing with S-containing functional groups in N/S doped microporous carbon. The uniform changes in the distribution and mass transfer of S and Pb, the non-uniform changes of N and Pb showed by TEM-EDS and the existence of PbS showed by XPS proved the above conclusion (Figs. 4b and c). In addition, as shown in Fig. S8, the adsorption capacity of N/S co-doped microporous carbon for Pb^{2+} was much greater than that of porous carbon without S doped, indicating that the S functional group rather than oxygen-containing functional group played promoting role in Pb^{2+} adsorption. According to previous studies, N/S doped microporous carbons exhibited stronger adsorption efficiency for Pb^{2+} than porous carbon in water and its adsorption equilibrium time was only 60 min (Jia et al. 2021). Therefore, it was concluded that the excellent adsorption capacity of Pb^{2+} on the N/S co-doped microporous carbon might be attributed to the the S containing functional groups toward Pb^{2+}. Further, a positive correlation was observed between O/C and Pb^{2+}-q_m (Fig. 4d), it revealed that carbonaceous precursor with high O/C was suitable for the preparation of N/S co-doped microporous carbon with strong adsorption capacity for Pb^{2+}.

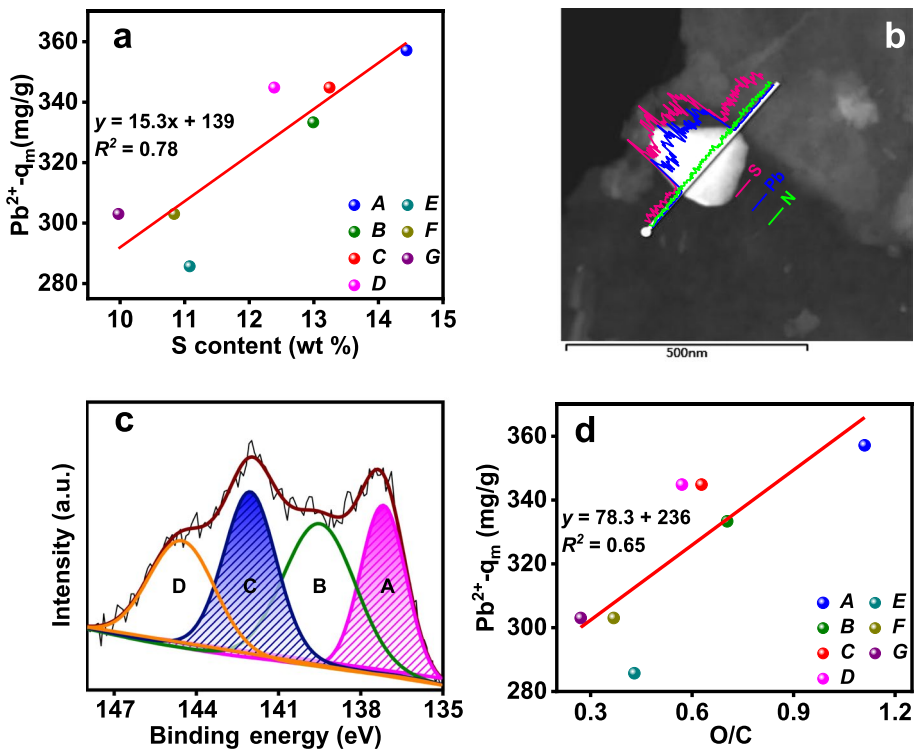

Fig. 4 **a** Linear correlation between Pb^{2+} maximum adsorption capacity (Pb^{2+}-q_m) and S content of N/S doped microporous carbon, **b** representative TEM-EDS line profiles of elements in the selected *NSC-CL* (derived from cellulose activated by KSCN) after Pb^{2+} adsorption, **c** XPS profiles of PbS in the selected *NSC-CL* after Pb^{2+} adsorption, A: PbS (Pb $4f^{7/2}$), B: $PbSO_3$ (Pb $4f^{7/2}$), C: PbS (Pb $4f^{5/2}$), D: $PbSO_3$ (Pb $4f^{5/2}$) and **d** linear correlation between O/C of carbonaceous precursors and Pb^{2+} maximum adsorption capacity (Pb^{2+}-q_m) of N/S co-doped microporous carbon (*A*: *NSC-CL*, *B*: *NSC-WS*, *C*: *NSC-SD*, *D*: *NSC-H-180*, *E*: *NSC-N-300*, *F*: *NSC-A-300*, *G*: *NSC-H-300*)

According to the above discussion, the developed microporous structure and high N doping in N/S co-doped microporous carbon were conducive to adsorb BPA, while the high S doping promoted Pb^{2+} adsorption. Meanwhile, the thermal stability and polarity of carbonaceous precursor control the microporous structure and N/S doping content of N/S doped microporous carbon, respectively. Therefore, it can be further concluded that the adsorption capacity of N/S co-doped microporous carbon for BPA and Pb^{2+} can be predicted directly by the properties of carbonaceous precursor. The carbonaceous precursor with high thermal stability was suitable for preparing N/S co-doped microporous carbon with strong adsorption capacity for BPA, and the carbonaceous precursor with high O/C was suitable for preparing N/S co-doped microporous carbon with strong adsorption capacity for Pb^{2+}.

4 Conclusion

In the present study, we found that the thermal stabilization effect and oxygen replacement reaction during the activation of carbonaceous precursor by KSCN significantly regulated the microporosity (express by surface area density and micropore surface area) and N/S doping ability of N/S doped microporous carbon. Results confirmed that the carbonaceous precursor with high R_{50} index occurred strong thermal stabilization effect during activated by KSCN, which produced more micropores. The carbonaceous precursor with high O/C occurred strong oxygen replacement reaction in the process of being activated by KSCN, which increased the S content. Further, high micropore surface area was essential for improving the BPA adsorption ability and high S doping was essential for improving the Pb^{2+} adsorption ability. In summary, the carbon material suitable for organic pollutants adsorption derived from the carbon precursor with high R_{50} index, while the carbon material with high adsorption capacity for Pb^{2+} derived from the carbon precursor with high O/C. Our results provided new insights into the directional, predictable and controllable activation of carbon materials, and provided a new way to solve the challenges of microporous material development.

Supplementary Information

The online version contains supplementary material available at https://doi.org/10.1007/s44246-022-00006-4.

Additional file 1: Table S1. N/S content of different carbonaceous precursors. **Fig. S1.** (a) N_2 adsorption-desorption isotherms and (b) pore size distribution of the N/S co-doped microporous carbon (*A*: *NSC-CL*, *B*: *NSC-WS*, *C*: *NSC-SD*, *D*: *NSC-H-180*, *E*: *NSC-N-300*, *F*: *NSC-A-300*, *G*: *NSC-H-300*). **Fig. S2.** (a) I_D/I_G values (obtained by fitting Raman spectra) of N/S co-doped microporous carbon produced by carbonaceous precursors with different R_{50} index and (b) linear correlation between R_{50} of carbonaceous precursors and micropores surface area of N/S co-doped microporous carbon (*A*: *NSC-CL*, *B*: *NSC-WS*, *C*: *NSC-SD*, *D*: *NSC-H-180*, *E*: *NSC-N-300*, *F*: *NSC-A-300*, *G*: *NSC-H-300*). **Fig. S3.** O1s XPS spectra for N/S co-doped microporous carbon derived from cellulose. **Fig. S4.** N1s XPS spectra for various N/S co-doped microporous carbon (N1: pyridinic N, N2: pyrrolic N, N3: quaternary N, N4: oxidic N). **Fig. S5.** (a) Adsorption kinetics of BPA onto N/S dope microporous carbon and (b) adsorption isotherms of BPA for N/S co-doped microporous carbon in aqueous solution (the adsorption isotherms were fitted with the Langmuir mdel) (*A*: *NSC-CL*, *B*: *NSC-WS*, *C*: *NSC-SD*, *D*: *NSC-H-180*, *E*: *NSC-N-300*, *F*: *NSC-A-300*, *G*: *NSC-H-300*). **Table S2.** The isothermal parameters and kinetic parameters of N/S co-doped microporous carbon for BPA adsorption. **Fig. S6.** Relationship between N_{BET} and BPA-q_{BET} (N_{BET} = N content/ BET surface area, suggesting N content per BET surface area. BPA-q_{BET} = q_m/BET surface area, suggesting BPA adsorption capacity per BET surface area, *A*: *NSC-CL*, *B*: *NSC-WS*, *C*: *NSC-SD*, *D*: *NSC-H-180*, *E*: *NSC-N-300*, *F*: *NSC-A-300*, *G*: *NSC-H-300, PC-1* and *PC-2*: porous carbon without N and S). **Fig. S7.** Adsorption isotherms of Pb^{2+} for N/S co-doped microporous carbon in aqueous solution (the adsorption isotherms were fitted with the Langmuir model, *A*: *NSC-CL*, *B*: *NSC-WS*, *C*: *NSC-SD*, *D*: *NSC-H-180*, *E*: *NSC-N-300*, *F*: *NSC-A-300*, *G*: *NSC-H-300*). **Table S3.** The Langmuir fitted isothermal parameters of N/S co-doped microporous carbon for Pb^{2+} adsorption. **Fig. S8.** Adsorption capacity of Pb^{2+} of N/S undoped and N/S doped carbon (the data of PC and CAC refer to the previous article (Jia et al. 2021), *A*: *NSC-CL*, *B*: *NSC-WS*, *C*: *NSC-SD*, *D*: *NSC-H-180*, *E*: *NSC-N-300*, *F*: *NSC-A-300*, *G*: *NSC-H- 300*).

Acknowledgements
Not applicable.

Authors' contributions
Conceptualization, Z.X.D., J.C. and S.S.S.; Formal analysis, S.S.S.; Funding acquisition, Z.X.D.; Investigation, S.S.S and H.X.Y.; Supervision, Z.S.C. and Z.X.D.; Writing—original draft, S.S.S.; Writing—review and editing, Z.X.D., Z.S.C. and X.Q.J. All authors have read and agreed to the published version of the manuscript.

Funding
Funding was provided by the National & Local Joint Engineering Laboratory for Municipal Sewage Resource Utilization Technology, Suzhou University of Science and Technology (No. 2021KF03) and Shanghai Natural Science Foundation (NO.19ZR1403800).

Availability of data and materials
The datasets used or analyzed during the current study are available from the corresponding author on reasonable request.

Declarations

Competing interests
The authors declare no competing financial interest.

Author details
[1]College of Environmental & Chemical Engineering, Shanghai University of Electric Power, Shanghai 200090, China. [2]Shanghai Technical Service Platform for Pollution Control and Resource Utilization of Organic Wastes, Shanghai Key Laboratory of Atmospheric Particle Pollution and Prevention (LAP3), Department of Environmental Science and Engineering, Fudan University, Shanghai 200438, China. [3]Shanghai Institute of Pollution Control and Ecological Security, Shanghai 200092, China. [4]National & Local Joint Engineering Laboratory for Municipal Sewage Resource Utilization Technology, Suzhou University of Science and Technology, Suzhou 215009, China.

Received: 17 March 2022 Accepted: 2 May 2022
Published online: 18 June 2022

References

Adeleye AT, Akande AA, Odoh CK, Philip M, Fidelis TT, Amos PI, Banjoko OO (2021) Efficient synthesis of bio-based activated carbon (AC) for catalytic systems: a green and sustainable approach. J Ind Eng Chem 96:59–75. https://doi.org/10.1016/j.jiec.2021.01.044

Ahamad T, Naushad M, Ruksana, Alhabarah AN, Alshehri SM (2019) N/S doped highly porous magnetic carbon aerogel derived from sugarcane bagasse cellulose for the removal of bisphenol A. Int J Biol Macromol 132:1031–1038. https://doi.org/10.1016/j.ijbiomac.2019.04.004

Alsewaileh AS, Usman AR, Al-Wabel MI (2019) Effects of pyrolysis temperature on nitrate-nitrogen (NO_3^--N) and bromate (BrO_3^-) adsorption onto date palm biochar. J Environ Manag 237:289–296. https://doi.org/10.1016/j.jenvman.2019.02.045

Altwala A, Mokaya R (2020) Predictable and targeted activation of biomass to carbons with high surface area density and enhanced methane storage capacity. Energy Environ Sci 13:2967–2978. https://doi.org/10.1039/d0ee01340d

Balahmar N, Al-Jumialy AS, Mokaya R (2017) Biomass to porous carbon in one step: directly activated biomass for high performance CO_2 storage. J Mater Chem A 5:12330–12339. https://doi.org/10.1039/c7ta01722g

Balahmar N, Mokaya R (2019) Pre-mixed precursors for modulating the porosity of carbons for enhanced hydrogen storage: towards predicting the activation behaviour of carbonaceous matter. J Mater Chem A 7:17466–17479. https://doi.org/10.1039/C9TA06308k

Gao S, Li L, Geng K, Wei X, Zhang S (2015) Recycling the biowaste to produce nitrogen and sulfur self-doped porous carbon as an efficient catalyst for oxygen reduction reaction. Nano Energy 16:408–418. https://doi.org/10.1016/j.nanoen.2015.07.009

Harvey OR, Kuo LJ, Zimmerman AR, Louchouarn P, Amonette JE, Herbert BE (2012) An index-based approach to assessing recalcitrance and soil carbon sequestration potential of engineered black carbons (biochars). Environ Sci Technol 46:1415–1421. https://doi.org/10.1021/es2040398

Hirst EA, Taylor A, Mokaya R (2018) A simple flash carbonization route for conversion of biomass to porous carbons with high CO_2 storage capacity. J Mater Chem A 6:12393–12403. https://doi.org/10.1039/C8TA04409K

Hu Y, Ma R, Ju Q, Guo B, Yang M, Liu Q, Wang J (2020) S, N dual-doped porous carbon materials derived from biomass for Na ion storage and O_2 electroreduction. Micropor Mesopor Mater 294:109930–109937. https://doi.org/10.1016/j.micromeso.2019.109930

Jia C, Yu F, Luo J, Chen C, Zhang S, Zhu X (2021) Three birds with one stone approach to superior N/S co-doped microporous carbon for gas storage and water purification. Chem Eng J 431:133231–133238. https://doi.org/10.1016/j.cej.2021.133231

Kasera N, Kolar P, Hall SG (2022) Nitrogen-doped biochars as adsorbents for mitigation of heavy metals and organics from water: a review. Biochar 4:17–47. https://doi.org/10.1007/s42773-022-00145-2

Liang J, Jiao Y, Jaroniec M, Qiao SZ (2012) Sulfur and nitrogen dual-doped mesoporous graphene electrocatalyst for oxygen reduction with synergistically enhanced performance. Angew Chem Int Ed Engl 51:11496–11500. https://doi.org/10.1002/anie.201206720

Lu K, Hao N, Meng X, Luo Z, Tuskan GA, Ragauskas AJ (2019) Investigating the correlation of biomass recalcitrance with pyrolysis oil using poplar as the feedstock. Bioresour Technol 289:121589–121595. https://doi.org/10.1016/j.biortech.2019.121589

Luo J, Jia C, Shen M, Zhang S, Zhu X (2019) Enhancement of adsorption and energy storage capacity of biomass-based N-doped porous carbon via cyclic carbothermal reduction triggered by nitrogen dopants. Carbon 155:403–409. https://doi.org/10.1016/j.carbon.2019.08.075

Ma W, Wang N, Du Y, Xu P (2019) Human-hair-derived N, S-doped porous carbon: an enrichment and degradation system for wastewater remediation in the presence of peroxymonosulfate. ACS Sustain Chem Eng 7:2718–2727. https://doi.org/10.1021/acssuschemeng.8b05801

Maliutina K, Huang J, Su T, Yu J, Fan L (2021) Biomass-derived Ta,N,S co-doped CNTs enriched carbon catalyst for efficient electrochemical oxygen reduction. J Alloys Compd 888:161479–161490. https://doi.org/10.1016/j.jallcom.2021.161479

Sun S, Han F, Wu X, Fan Z (2020) One-step synthesis of biomass derived O, N-codoped hierarchical porous carbon with high surface area for supercapacitors. Chin Chem Lett 31:2235–2238. https://doi.org/10.1016/j.cclet.2019.11.023

Tan H, Liu J, Huang G, Qian Y, Deng Y, Chen G (2018) Understanding the roles of sulfur doping for enhancing of hydrophilicity and electrochemical performance of N,S-codoped hierarchically porous carbon. Appl Energy Mater 1:5599–5608. https://doi.org/10.1021/acsaem.8b01131

Teong CQ, Setiabudi HD, El-Arish NAS, Bahari MB, Teh LP (2021) Vatica rassak wood waste-derived activated carbon for effective Pb(II) adsorption: kinetic, isotherm and reusability studies. Mater Today Proc 42:165–171. https://doi.org/10.1016/j.matpr.2020.11.270

Tian W, Zhang H, Duan X, Sun H, Tade MO, Ang HM, Wang S (2016a) Nitrogen- and sulfur-codoped hierarchically porous carbon for adsorptive and oxidative removal of pharmaceutical contaminants. ACS Appl Mater Inters 8:7184–7193. https://doi.org/10.1021/acsami.6b01748

Tian W, Zhang H, Sun H, Suvorova A, Saunders M, Tade M, Wang S (2016b) Heteroatom (N or N-S)-doping induced layered and honeycomb microstructures of porous carbons for CO_2 capture and energy applications. Adv Funct Mater 26:8651–8661. https://doi.org/10.1002/adfm.201603937

Xiong Z, Huanhuan Z, Jing W, Wei C, Yingquan C, Gao X, Haiping Y, Hanping C (2021) Physicochemical and adsorption properties of biochar from biomass-based pyrolytic polygeneration: effects of biomass species and temperature. Biochar 3:657–670. https://doi.org/10.1007/s42773-021-00102-5

Zhou J, Shen H, Li Z, Zhang S, Zhao Y, Bi X, Wang Y, Cui H, Zhuo S (2016) Porous carbon materials with dual N, S-doping and uniform ultra-microporosity for high performance supercapacitors. Electrochim Acta 209:557–564. 10:5840-5848. https://doi.org/10.1021/es500531c

Zhu X, Liu Y, Luo G, Qian F, Zhang S, Chen J (2014a) Facile fabrication of magnetic carbon composites from hydrochar via simultaneous activation and magnetization for triclosan adsorption. Environ Sci Technol 48:5840–5848. https://doi.org/10.1021/es500531c

Zhu X, Liu Y, Qian F, Zhou C, Zhang S, Chen J (2015) Role of hydrochar properties on the porosity of hydrochar-based porous carbon for their sustainable application. ACS Sustain Chem Eng 3:833–840. https://doi.org/10.1021/acssuschemeng.5b00153

Zhu X, Liu Y, Zhou C, Zhang S, Chen J (2014b) Novel and high-performance magnetic carbon composite prepared from waste hydrochar for dye removal. ACS Sustain Chem Eng 2:969–977. https://doi.org/10.1021/sc400547y

Publisher's Note